

## Effect of graphene oxide doping on anti-/deicing performance of shape memory epoxy resin

4 Long Chen<sup>a,b,c,\*</sup>, Yeqin Shen<sup>a,b</sup>, Zhanqiang Liu<sup>a,b</sup>, Qinghua Song<sup>a,b</sup>, Chaozong Liu<sup>d</sup>

5 (<sup>a</sup> Key Laboratory of High Efficiency and Clean Mechanical Manufacture, Ministry of Education, Jinan,  
6 China

7 <sup>b</sup> School of Mechanical Engineering, Shandong University, Jinan, China

8 <sup>c</sup> Shenzhen Research Institute of Shandong University, Shenzhen, China

9 <sup>d</sup> Institute of Orthopaedic & Musculoskeletal Science, University College London, London, United Kingdom)

10

11 **Abstract:** Shape memory GO/EP composites with different fractions of  
12 GO were prepared by thermal curing. The glass transition temperature  
13 was measured and the shape memory performance experiments were  
14 performed. The experimental results shows that with the increasing of  
15 GO contents, the shape retention ratio of the shape memory GO/EP  
16 composites with 1.25 wt% GO content decreased by 8.40%, while the  
17 shape recovery ratio increased by 16.26%. The experimental data were  
18 analyzed by molecular dynamics (MD) simulation that the chemical bond  
19 between the GO layer and the EP molecule is the reason for improving  
20 the shape memory performance. In addition, it was found through MD  
21 simulation that the agglomeration of GO reduces the recovery  
22 performance of the shape memory GO/EP composites. When GO content  
23 was 10 wt%, the recovery performance of GO agglomerated composites  
24 was 14.38% lower than that of GO uniformly dispersed, and 3.30% lower

25 than that of pure shape memory EP. Through the combination of  
26 experiment and calculation, a new idea for the design of shape memory  
27 GO/EP composites was provided.

28

29 **Key words:** Shape memory, Graphene oxide, Polymer, Thermodynamic,  
30 Molecular dynamics simulation

31

## 32 **1. Introduction**

33 Shape memory material is a special material that can produce shape  
34 recovery by external stimulus [1]. Common stimuli are heat [2-3], electric  
35 field [4-5], magnetic field [6-7], acid-base [8], and other external stimulus  
36 [9-10]. As an emerging polymer material, shape memory polymer has a  
37 wide range of applications in aerospace [11], medical [12-13], and  
38 industrial manufacturing [14]. Common shape memory polymers include  
39 polycaprolactone diol [15], epoxy resin [16], polyurethane [17], etc.  
40 These polymers have high glassy-rubbery modulus, thereby producing  
41 shape memory effects. Therefore, the shape memory epoxy resin material  
42 can be used for the anti-/deicing of the aircraft.

43 However, pure shape memory polymers also have certain  
44 shortcomings and limitations [18], including lower recovery speed and  
45 lower recovery ratio [19]. Therefore, different types of carbon  
46 nanoparticles, such as carbon nanotubes [20-21], graphene [22], nanoclay

47 [23], and metals or metal oxides [24] have been employed to improve  
48 shape memory performance [25].

49 GO is a compound composed of graphene and functional groups  
50 (such as hydroxyl and carboxyl), and has physical properties similar to  
51 graphene [26-27], including high Young's modulus (1.0 TPa) [28] and  
52 high thermal conductivity ( $\sim 5000 \text{ W(m}\cdot\text{K)}$ ) [29]. GO is widely added as  
53 a filler in polymers [30-31]. A tremendous amount of research have  
54 shown that introducing GO to polyurethane can significantly increase the  
55 elastic modulus and shape recovery rate [32,33,35]. In addition, adding  
56 GO filler can effectively improve the thermal response recovery rate of  
57 shape memory epoxy resin [34]. Kim et al. [32] introduced 1.5 wt% of  
58 GO to acrylate-terminated polyurethane isocyanate and found that the  
59 shape memory performance was improved by 1%. Luo et al. [33] added  
60 GO to polyurethane and kept it at 80 °C for 4 hours to obtain a  
61 Polyurethane/GO composite with self-healing properties and shape  
62 memory properties. The modulus was increased by 147.2%, and the  
63 shape recovery ratio reached 88.6%. Xu et al. [34] indicated that adding  
64 VGCF-GO filler can effectively improve the thermal response recovery  
65 ratio of EP with less than about 10% strain during the stretching process.  
66 Under the pre-strain was 10%, the maximum thermal response recovery  
67 ratio of the GO doped composite increased by 22%. Hhosh et al. [35]  
68 added reduced graphene oxide (RGO) to the polyurethane-polystyrene

69 material, and the samples show that the shape recovery ratio reaches  
70 265~308 % within 33~44 s under microwave stimulation.

71 In recent years, molecular dynamics simulation has been widely  
72 employed to investigate the performance improvement mechanism of  
73 shape memory polymers. Molecular dynamics simulation can analyze the  
74 effect of GO doping on the shape memory performance of shape memory  
75 epoxy resin from the perspective of molecular stretching, intermolecular  
76 energy and bonding [36-39]. Wick et al. [36] conducted molecular  
77 dynamics simulations on isophorone diamine shape memory EP and the  
78 results show that the higher the cross-linking percentage, the higher the  
79 bond energy stored by the epoxy resin molecules under the stretching of  
80 50 %. Yang et al. [37] combined a covalent adaptive network with a shape  
81 memory polymer for molecular dynamics simulation and found that as  
82 the end-to-end distance of the polymer chain decreases, the Diels-Alder  
83 network exhibits higher flexibility, which greatly improves the  
84 mechanical and shape memory performance. Zhang et al. [38] found that  
85 the molecular bonding between GO and EP is the key to enhancing the  
86 shape memory performance through molecular dynamics simulation of  
87 shape memory GO/EP composites. The reinforcing effect of graphene on  
88 the shape memory epoxy from the perspective of molecular entropy and  
89 energy was explained by Amini et al. [39]. With the addition of GO, the  
90 energy stored in the shape memory epoxy increases, which improves the

91 recovery performance.

92 In this paper, the shape memory GO/EP composites with different  
93 graphene oxide mass fractions were successfully prepared. The glass  
94 transition temperature, shape fixation ratio, and shape recovery ratio were  
95 determined. The recovery process curve of shape memory GO/EP  
96 material was presented, and the effect of GO on enhancing the shape  
97 memory performance was explained. Moreover, the molecular dynamics  
98 simulation was established to investigate the influence of the molecular  
99 interaction between GO and EP on the shape memory performance, and  
100 the influence of the distribution of GO on the shape memory performance  
101 of the composites from a microscopic point of view.

## 102 **2. Experimental section**

### 103 *2.1 Preparation of shape memory GO/EP composites*

#### 104 *2.1.1 Materials*

105 The multilayer GO with a purity of 95% and thickness of 3.4~7 nm  
106 was provided by Suzhou Hengqiu Technology Co., Ltd., Suzhou, China.  
107 The GO has the properties with a layer diameter of 10~50  $\mu\text{m}$ , number of  
108 layers 5~10, a specific surface area of 100~300  $\text{m}^2/\text{g}$ , and a sulfur content  
109 of <5 wt%. The manufacturer of epoxy resin E-51 was Shanghai Aotun  
110 Chemical Technology Co., Ltd., Shanghai, China. The epoxy value is  
111 184~195 g/mol, the viscosity is 10000~16000 mPa s, the color degree is  
112 less than 40 Pt-Co, and the degree of hydrolysis is less than 0.5%. The

113 curing agent DDM was purchased from Shanghai Zhanyun Chemical Co.,  
114 Ltd., Shanghai, China, with a molecular weight of 198.26, a melting point  
115 range of 89.0~93.2 °C.

### 116 *2.1.2 Preparation process*

117 As shown in Figure 1, 6ml ethanol was added to the beaker, and the  
118 multilayer GO powder was weighed according to the percentage of the  
119 mass of EP as shown in Table 1. The mixture was dispersed ultrasonically  
120 for 15 minutes. 30g of epoxy resin was add to another beaker and put into  
121 the water bath preheat to 80 °C for 10 min, then pour the dispersed GO  
122 into the preheated EP. The mixed beaker was placed in an ultrasonic  
123 disperser for ultrasonic dispersion for 30 min. The beaker was heated at  
124 90 °C for 2 hours in the blast drying oven. After the process, the beaker  
125 was moved in a magnetic water bath heating stirrer, which has been  
126 preheated to 90 °C, and the epoxy resin mixture is evenly stirred. In order  
127 to have shape memory function after molding, it should not be completely  
128 cured that 5.1g curing agent DDM was used. The curing agent was  
129 introduced into the beaker containing EP step by step and stirred for 10  
130 minutes until the bubbles disappeared. Finally, the evenly stirred mixtures  
131 were poured into the mold, and put it into the blast oven. The curing was  
132 at 80 °C for 2.5 hours and then 150 °C for 2.0 hours.

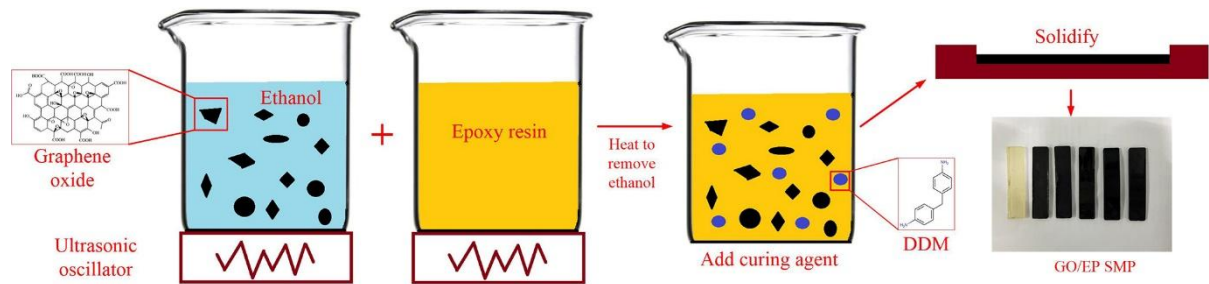


Fig. 1. Preparation of shape memory GO/EP composites.

Table 1. The content of each material in the composite material

	EP (g)	GO (g)	DDM (g)
Shape memory EP	30	0	5.1
GO/EP-0.10 wt%	30	0.03	5.1
GO/EP-0.25 wt%	30	0.075	5.1
GO/EP-0.50 wt%	30	0.150	5.1
GO/EP-1.00 wt%	30	0.300	5.1
GO/EP-1.25 wt%	30	0.375	5.1

## 2.2 Characterization and measurements

### 2.2.1 Scanning electron microscope (SEM)

SEM characterization (FEI-QUANTA FEG 250) was performed on the prepared shape memory GO/EP composite samples. The dispersion of GO in EP matrix was observed according to the cross-sectional images of the shape memory GO/EP composites by SEM scanning. Furthermore, SEM images show that there are no visible holes or cracks in the samples, which reflects the adhesion between GO and EP.

### 2.2.2 Glass transition temperature measurement

The DSC (TA Instrument-DSC 2500) with power compensation was used for the glass transition temperature ( $T_g$ ) measurement. The supporter of the sample and the reference are independent components. There is a platinum thermistor for heating and a platinum sensor for temperature

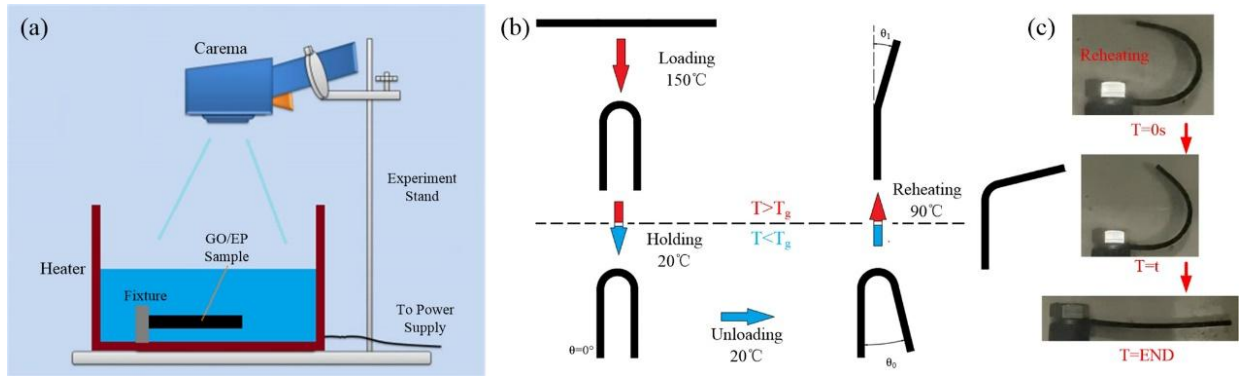
149 measurement at the bottom of the sample and the reference. According to  
150 the principle of dynamic zero balance, the temperature of the sample and  
151 the reference material should be kept in the dynamic zero balance state  
152 whether the sample is endothermic or exothermic. Therefore, the DSC  
153 curve was obtained by heating the sample to 200 °C and then cooling it at  
154 the ratio of 10 °C/min. The DSC measures the energy difference  
155 ( $\Delta W=dH/dt$ ) required to maintain the sample and the reference at the  
156 same temperature, which reflects the change of the sample enthalpy.  
157 From the point of view of molecular motion, the glass transition is related  
158 to the micro-Brownian motion of the molecular segments in the  
159 amorphous part of amorphous polymer or crystalline polymer. Below the  
160  $T_g$ , the movement of the shape memory EP is basically frozen. After  
161 reaching the  $T_g$ , the active wave heat capacity of the shape memory EP  
162 increases, and the baseline moves to the endothermic side.

### 163 *2.3 Shape fixity ratio and shape recovery ratio*

164 The prepared shape memory GO/EP composites sample (Size  
165 90×20×4 mm) was placed in a blast drying oven at 150 °C for 10 minutes.  
166 The sample was taken out and bent in the mold, and kept until the sample  
167 cooled to room temperature to record the bending angle. As shown in  
168 Figure 2(a), the sample was placed in a water bath heater and heated at  
169 90 °C. Then the sample was photographed and the bending angle was  
170 recorded every 10 s. Figure 2(b) shows the angle change process of the



171 experimental sample. After the sample was bent and fixed in the mold,  
 172 the mold was removed and the sample was cooled to room temperature.  
 173 The sample had a small recovery angle, which was set as  $\theta_0$ . This state  
 174 was regarded as the initial state of the experiment. When the sample was  
 175 placed in the water bath heater, the angle will continue to recover, but it  
 176 will not recover completely in the end. The sample angle of the final state  
 177 was set as  $\theta_1$ . Figure 2(c) shows the recovery process of the shape  
 178 memory GO/EP composites.



179 Figure 2. Schematic of (a) experimental device, (b) thermal cycle, and (c) recovery process.  
 180

181 The shape fixity ratio refers to the shape retention of the shape  
 182 memory material at room temperature after it is heated and deformed.

183 The shape fixity ratio  $R_F$  is calculated by Equation (1) [39].

$$R_F = \frac{180^\circ - \theta_0}{180^\circ} \quad (1)$$

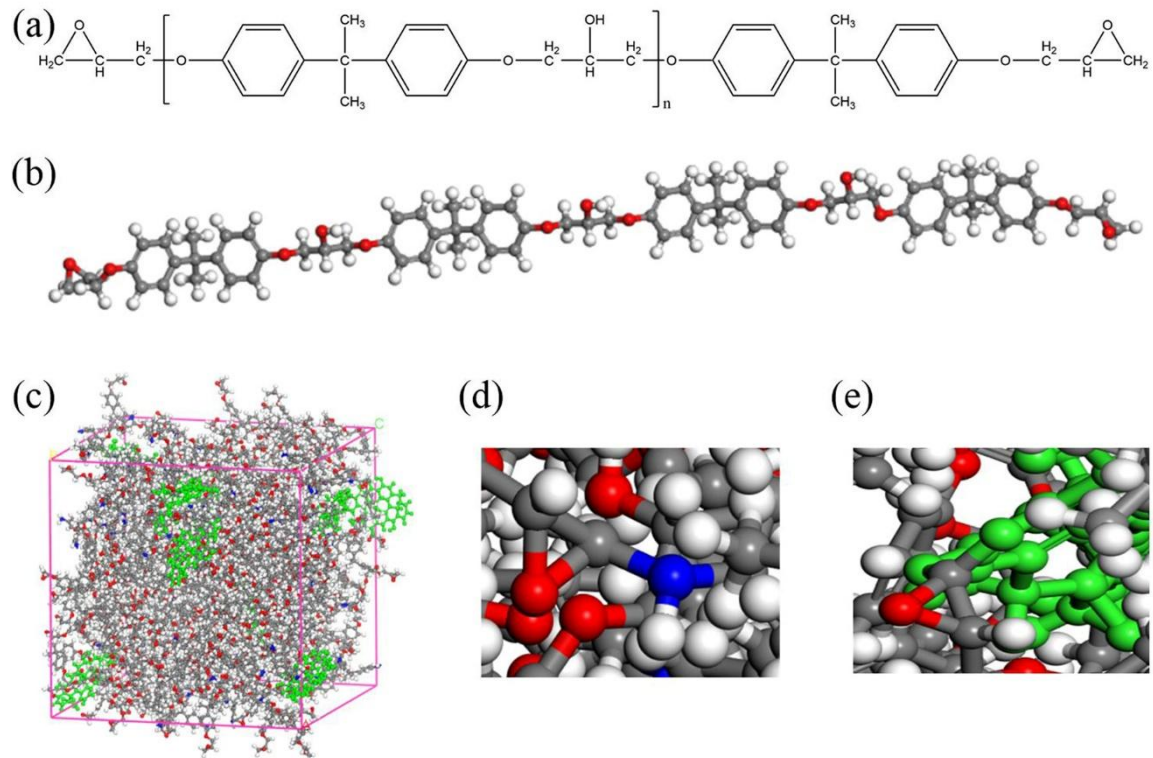
184 The shape recovery ratio represents the deformation recovery of the  
 185 shape memory GO/EP composites after deformed and cooled. The shape  
 186 recovery ratio  $R_V$  can be expressed as Equation (2).

$$R_v = \frac{180^\circ - \theta_1 - \theta_0}{180^\circ - \theta_0} \quad (2)$$

### 187 **3. Molecular dynamics analysis**

#### 188 *3.1 Simulation parameters*

189 In the molecular dynamic simulation, the E-51 polymer chain is  
190 synthesized from bisphenol A and epichlorohydrin (see Figure 3(a) and  
191 (b)). As shown in Figure 3(c), the model unit cell contains 200 polymer  
192 chains and 60 DDM molecules, which is represented as N-link. The  
193 connection ratio is 25% and the outermost carbon atoms of GO are  
194 partially oxidized to hydroxyl groups by passivating hydrogen (as shown  
195 in Figure 3(d)). Van der Waals force exists between the GO sheet and the  
196 EP, and there is a chemical bond between the GO functional group and  
197 the EP molecule. As shown in Figure 3(e), the bonding ratio is 100 %.  
198 The initial density is 1.5 g/cm<sup>3</sup>. The model size is 49.79×49.79×49.79 Å.  
199 Before the simulation, the model uses the Forceite module to minimize  
200 the energy under the NPT condition, and the force field is set as  
201 CAMPASS II to minimize the potential energy of the unit cell.



202  
 203 Figure 3. Schematic diagram of (a) E-51 molecular formula, (b) E-51 molecular model, (c) shape  
 204 memory GO/EP model, (d) cross-linking between EP and DDM, and (e) EP and GO bonding.

### 205 3.2 Validation of molecular dynamics model

206 The  $T_g$  was calculated by molecular dynamics and the correctness of  
 207 molecular dynamics simulation was verified by comparing the  
 208 experimental data with the simulation results [38]. In molecular dynamics  
 209 simulation, the relaxed structure of the shape memory EP unit cell was  
 210 heated to 500 K under NPT conditions, and balanced for 50 ps under the  
 211 pressure of 0.1 MPa. Then the heated structure was cooled to 300 K at a  
 212 cooling ratio of 2 K/ps under NPT conditions. The thermal expansion  
 213 formula is as follows [39].

$$3\alpha \cong \frac{1}{V_0} \frac{\partial V}{\partial T} = \rho_0 \frac{\partial V}{\partial T} \quad (3)$$

214 Where  $V_0$  and  $\rho_0$  denote the volume and density of the unit cell,  $\alpha$

215 denote the linear thermal expansion coefficient.

216 According to Equation (3), the specific volume change of shape  
217 memory GO/EP composites can be represented by a regression line. As  
218 shown in Figure 4, it can be seen that the specific volume-temperature  
219 curve has an obvious discontinuity. This discontinuity is due to the fact  
220 that the shape memory GO/EP composites are a glassy solid before  
221 reaching the glass transition temperature. After heating, the molecular  
222 fluidity is small, so the volume changes slowly and the specific volume  
223 changes quickly. While, when the temperature is higher than the glass  
224 transition temperature of shape memory GO/EP composites, the material  
225 presents rubber colloidal state and the fluidity increases greatly, so the  
226 volume changes rapidly and the specific volume changes slowly.  
227 Therefore, the intersection of the two regression lines is the glass  
228 transition temperature. The glass transition temperature of the SMP  
229 material shown in Figure 4 is 331 K and the error of the DSC experiment  
230 result is 3.33 %, which is within the allowable range of error, indicating  
231 that the molecular dynamics simulation results of the model are credible.

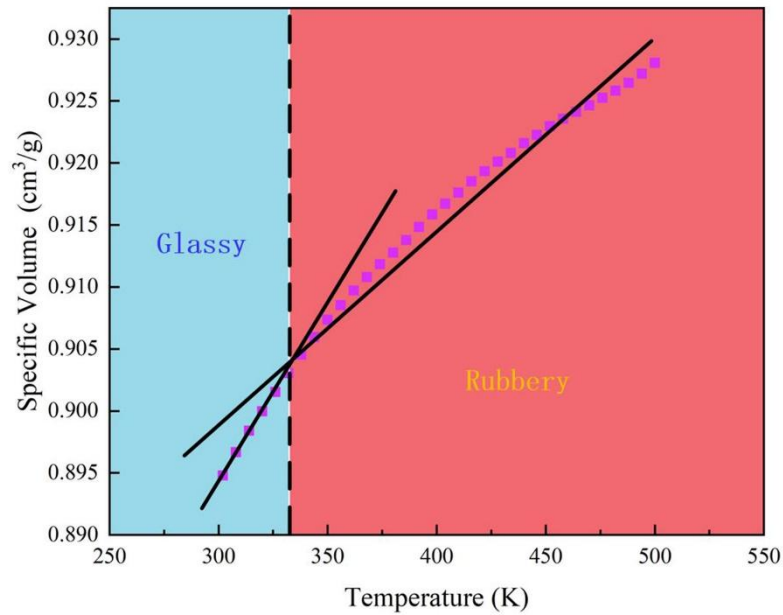
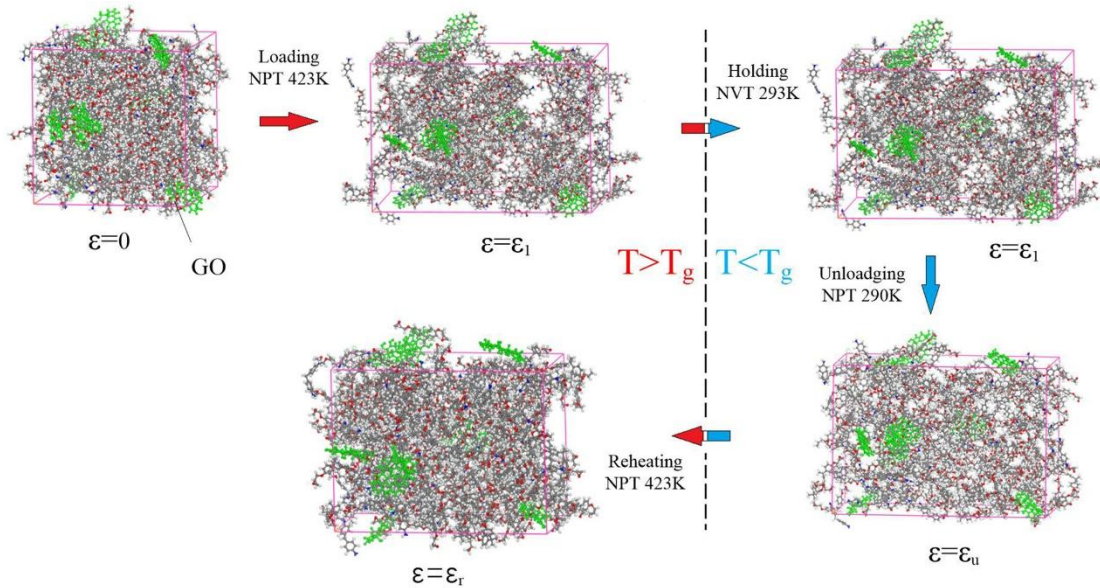


Figure 4. Specific volume-temperature diagram.

### 3.3 Shape recovery ratio

As shown in Figure 5, GO was embedded in the shape memory EP in a random distribution form in the unit cell. Thermal mechanical cycle simulation of unit cell was performed. The first step was to apply a stress of 1 GPa to the unit cell under the NPT conditions. The force field was set as CAMPASS II, and the Souza-Martins condition. The temperature was set as 423 K, and the duration is 5000 fs. During the process, the unit cell was stretched. The second part is to maintain the stress. The cell is cooled at 290 K for 5000 fs under NVT condition, and the cell length remains unchanged during the process. The third step is to remove the external force of NPT process, the temperature is 290 K for 5000 fs. In this process, the cell length will return to a small section. The last step is the reheat process. The temperature was set as 423 K for 30000 fs under

247 the NPT condition. During this process, the cell length will slowly  
248 recover.



249

250

Figure 5. Thermo-mechanical simulation process.

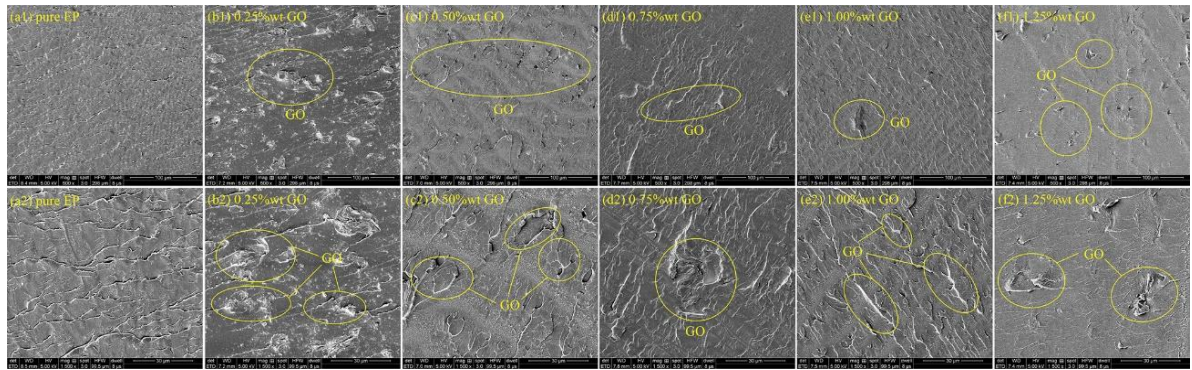
## 251 4. Results and discussion

### 252 4.1 Characterization

#### 253 4.1.1 SEM analysis

254 The SEM results were as shown in Figure 6. The yellow circle shows  
255 the GO layer. It can be seen that GO is evenly distributed in the EP matrix  
256 and there are no defects such as pores inside the sample, which indicating  
257 that the sample is well prepared. The use of ethanol can uniformly  
258 disperse GO in the EP matrix as much as possible, and the dispersibility  
259 of GO has a direct effect on the shape memory performance of the shape  
260 memory GO/EP composites.





261

262 Figure 6. SEM micrographs of the liquid nitrogen cryogenic fractured surfaces of the specimens.

263 (a1) and (a2) pure shape memory EP; (b1) and (b2) 0.25 wt% GO; (c1) and (c2) 0.50 wt% GO;

264 (d1) and (d2) 0.75 wt% GO; (e1) and (e2) 1.00 wt% GO; (f1) and (f2) 1.25 wt% GO.

#### 265 4.1.2 Glass transition temperature analysis

266 Figure 7 shows the DSC curves of shape memory GO/EP composites

267 with different GO contents. The determination of the glass transition

268 temperature is based on the deviation of the baseline on the DSC curve.

269 According to the standard committee of ICTA, the intersection of the

270 tangent line of the front edge of the curve and the front baseline is the

271 glass transition temperature. Thus the results of glass transition

272 temperature are shown in Table 2.

273

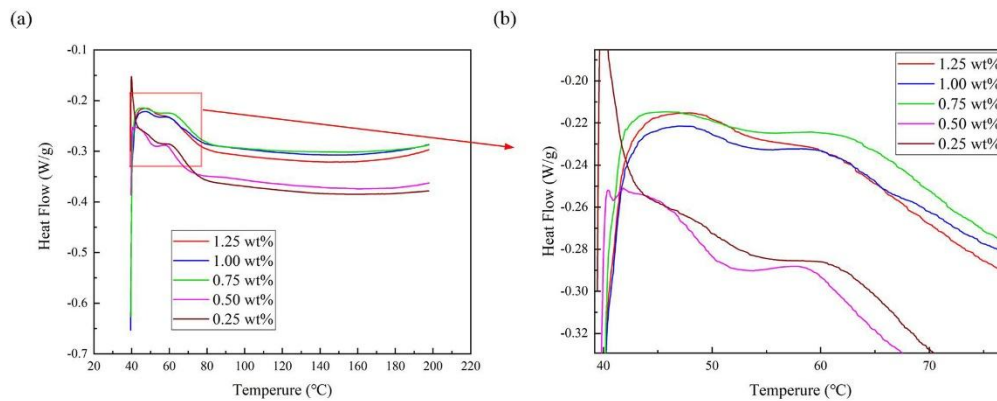
Table 2. Glass transition temperature values

GO contents (wt%)	T <sub>g</sub> (°C)
0	60.00
0.25	43.20
0.50	45.60
0.75	47.10
1.00	48.20
1.25	49.05

274

For pure shape memory EP, the glass transition temperature is 60 °C.

275 The glass transition temperature of the shape memory materials with GO  
276 is lower than 60 °C, and the glass transition temperature increases with  
277 the increase of GO content. The glass transition temperature of the shape  
278 memory GO/EP composites with 1.25 wt% is 10.95 °C lower than that of  
279 pure shape memory EP. However, compared that of shape memory  
280 GO/EP composites with 0.25 wt% GO doping, the glass transition  
281 temperature with 1.25 wt% was increased by 5.85 °C. The DSC results  
282 show that GO can reduce the glass transition temperature.



283

284

Figure 7. The DSC curves with different GO contents.

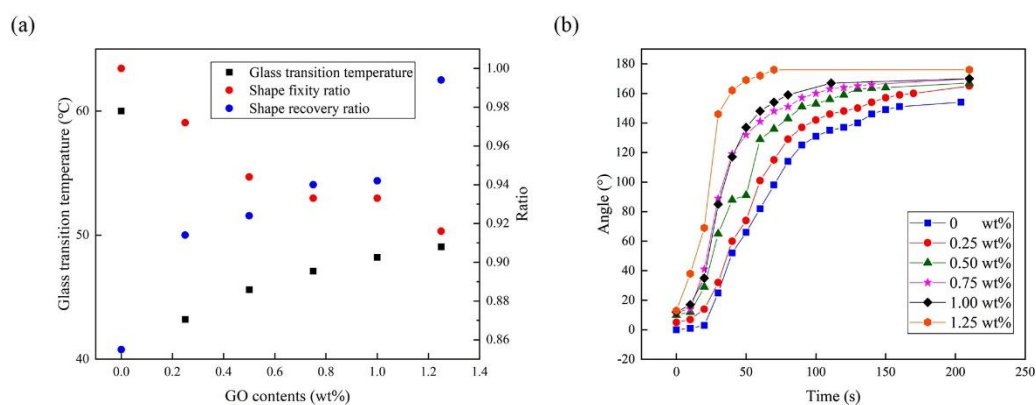
#### 285 4.3 Shape fixity ratio and shape recovery ratio analysis

286 It can be seen from Figure 8(a) that with the increase of GO content,  
287 the shape fixity ratio of shape memory GO/EP composites decreased. The  
288 shape fixity ratio of the shape memory material with GO content of 1.25  
289 wt% is 91.60%, which is 8.40% lower than that of the pure shape  
290 memory EP. With the increase of GO content, the shape recovery ratio of  
291 shape memory GO/EP composites shows an upward trend. The shape  
292 recovery ratio of the shape memory composites with GO content of 1.25



293 wt% is 99.40%, while the shape recovery ratio of the pure shape memory  
 294 EP is only 85.50%. Figure 8(b) shows the angle change of the shape  
 295 memory material with time. It can be seen from the figure that the shape  
 296 memory material with GO content of 1.25 wt% has recovered 79.60%  
 297 (reaching 133.00 °) in the first 30 s, while the shape recovery of the pure  
 298 shape recovery EP did not return to 131.00 ° until 160 s.

299 From Figure 8(b), it can be seen that with the increase of GO content,  
 300 the shape recovery speed of shape memory GO/EP composites increases  
 301 first and then decreases. The fast recovery interval of shape memory  
 302 GO/EP composites is ahead of time, and slow recovery area in the early  
 303 stage is shortened rapidly. When the GO content is 1.25 wt%, the rapid  
 304 recovery starts from the initial recovery time, which is 30 s earlier than  
 305 the pure shape memory EP.



306  
 307 Figure 8. (a) Glass transition temperature/shape fixity ratio/shape recovery ratio with GO contents,  
 308 and (b) Angle graph with time.

309 As shown in Figure 9, as the GO content increases, the angle of the  
 310 shape memory GO/EP composites at the end of the rapid recovery also  
 311 increases, and the angle of the shape memory GO/EP composites with the

312 GO content of 1.25wt% at the end of the rapid recovery is 162.00 °.

313 Moreover, the recovery completion time of shape memory GO/EP

314 composites also decreases rapidly with the increase of GO contents.

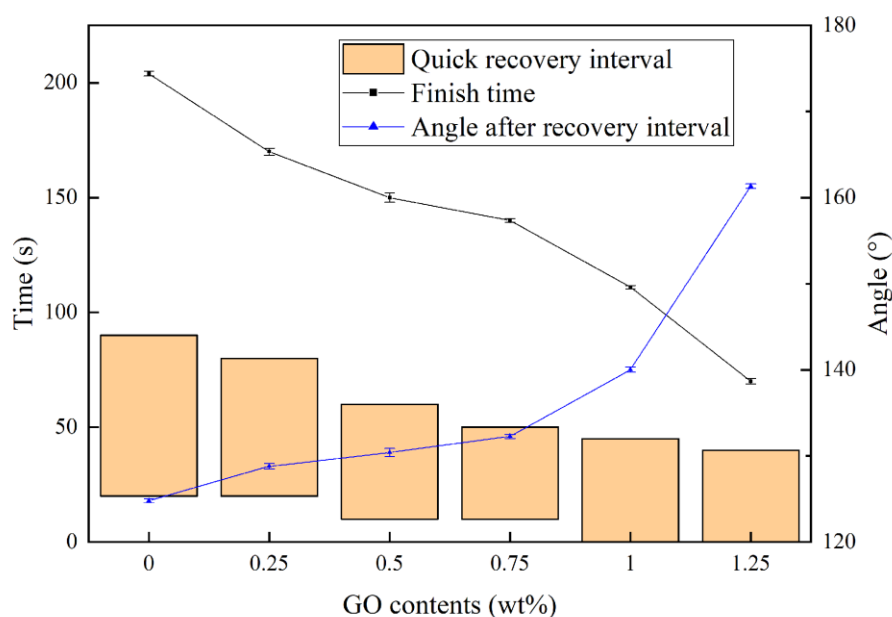
315 When the GO content is 1.25 wt%, it only takes 70 s to complete the

316 entire recovery process, while pure shape memory EP requires 204 s. It

317 shows that the addition of GO can promote the recovery of the shape

318 memory GO/EP composites, which shorting the total recovery time and

319 accelerating the recovery speed.



320

321

Figure 9. Quick reply interval and reply time.

#### 322 4.4 Molecular dynamics analysis

##### 323 4.4.1 Shape recovery ratio analysis

324 The shape recovery ratio refers to the ratio of the difference between

325 the strain after stretching ( $\epsilon_r$ ) and the strain after recovery is completed

326 ( $\epsilon_1$ ). Thus, the shape recovery ratio shown in Figure 5 can be expressed

327 by Equation (4) [39]:

$$\varepsilon_R = \frac{\varepsilon_1 - \varepsilon_r}{\varepsilon_1} \quad (4)$$

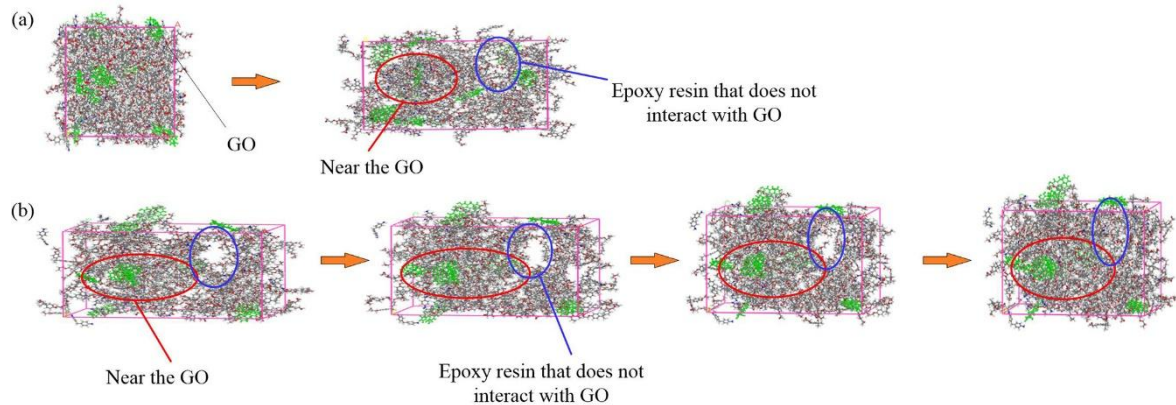
328 Converting the unit cell strain  $\varepsilon$  into the length  $L$ , the shape recovery  
329 ratio can be written as Equation (5) by the length after stretching ( $L_r$ ) and  
330 the length after recovery is completed ( $L_1$ ):

$$L_R = \frac{L_1 - L_r}{L_1} \quad (5)$$

331 As shown in Figure 10(a), during the stretching process, since the GO  
332 sheets cannot be stretched and deformed. Under the action of the  
333 intermolecular force between the GO and EP around the GO, the  
334 molecular distance of EP around GO will not be enlarged. The red circle  
335 in Figure 10(b) shows the EP molecules with recovery deformation  
336 around GO, and the blue circle shows the EP molecules without recovery  
337 deformation. It can be seen that the EP around the GO recovers faster,  
338 which is due to the intermolecular force generated between the GO sheet  
339 and the surrounding EP. The intermolecular force will promote the  
340 contraction of the molecular chain of the EP. This also explains the reason  
341 why the shape retention ratio decreases after GO doping.

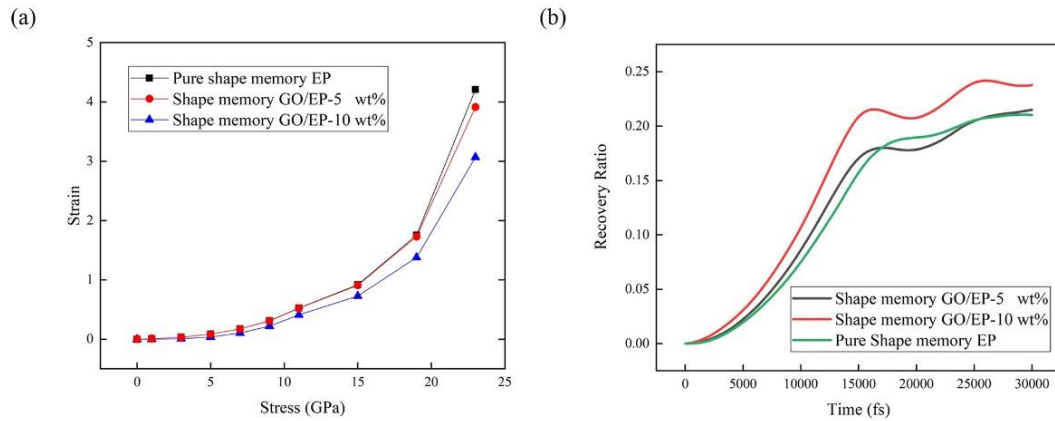
342 In addition, the thermal conductivity of the GO sheet is much higher  
343 than that of the shape memory EP. When the temperature of the epoxy  
344 resin near the GO sheet inside the composite is higher than other  
345 positions, this also promotes the shrinkage of the epoxy resin molecular

346 chain near the GO sheet. This also explains why the shape retention ratio  
347 of the material decreases after GO is introduced into the shape memory  
348 EP.



349  
350 Figure 10. (a) The stretching process and (b) recovery process of the unit cell.

351 According to the calculation of Equation (5), the recovery data were  
352 drawn in Figure 11(a). During the stretching process of the unit cell, the  
353 GO sheet will not be stretched and deformed under the action of  
354 intermolecular force between the GO and the EP around the GO. The  
355 molecular distance of EP around GO will not be excessively enlarged.  
356 Therefore, the strain of GO-EP is smaller than that of pure shape memory  
357 EP under the same stress. In the recovery process of unit cell, it can be  
358 seen that the unit cell with GO takes less time to reach the same strain  
359 than the unit cell of pure shape memory EP, and the rapid recovery  
360 interval is achieved earlier than that of pure shape memory EP, which is  
361 in accordance with the experimental results shown in Fig. 11(b).



362  
 363 Figure 11. (a) Stress-strain graph during stretching, and (b) strain versus time graph during  
 364 recovery.

#### 365 4.4.2 Influence of GO agglomeration

366 The uneven distribution or agglomeration of GO in shape memory EP  
 367 will directly affect the shape memory characteristics. Compared with the  
 368 uniformly dispersed unit cell (Figure 12(a)) and the agglomerated unit  
 369 cell (Figure 12(b)), it can be seen that when GO is uniformly dispersed,  
 370 the oxygen-containing functional groups at the edge and inside of GO  
 371 lamellae are fully combined with EP molecules. As shown in the red  
 372 circle in Figure 12(a), when GO agglomerations, the distance between  
 373 GO lamellae is significantly reduced, and the functional groups that GO  
 374 interact with EP molecules only exist at the edge of GO sheets. The  
 375 oxygen-containing functional groups in GO and part of the edge are  
 376 blocked, resulting in less EP molecules combined with GO than that of  
 377 GO is uniformly dispersed with the same mass fraction. Thus, the shape  
 378 recovery performance of the shape memory GO/EP composites is  
 379 reduced.

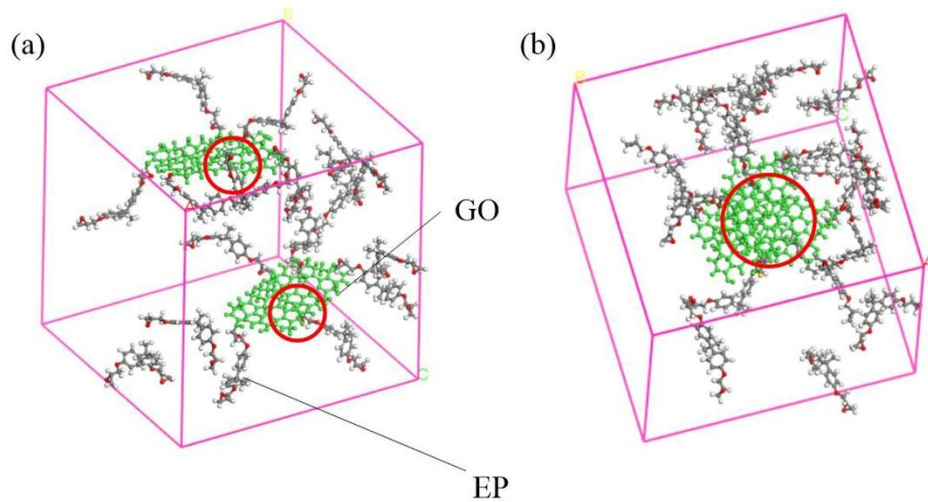


Figure 12. Unit cell of (a) GO uniform dispersion, and (b) GO agglomeration.

380  
381

382 It can be seen from Figure 13 that for shape memory GO/EP  
 383 composites with 10 wt% GO content, the shape recovery effect of GO  
 384 agglomeration is 14.38% lower than that of the GO uniformly dispersed  
 385 material. Moreover, compared with pure shape memory EP, the shape  
 386 recovery ratio is 3.30% lower and the recovery speed in the early stage is  
 387 slower than that of GO uniformly dispersed composites. With the increase  
 388 of GO mass fraction, the distribution of GO in the cell becomes denser  
 389 and the GO lamellar spacing is smaller, which is similar to agglomeration  
 390 and affects the shape recovery performance. For the material with GO  
 391 content of 15 wt%, the shape recovery ratio is further reduced to 20.34%,  
 392 which is 3.25% lower than that of the pure EP, and the initial recovery  
 393 ratio is also lower than that of the pure EP.

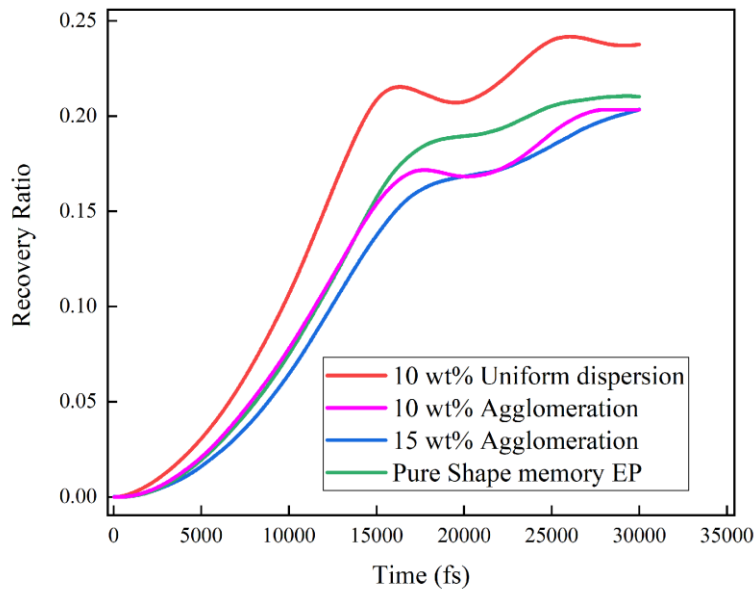
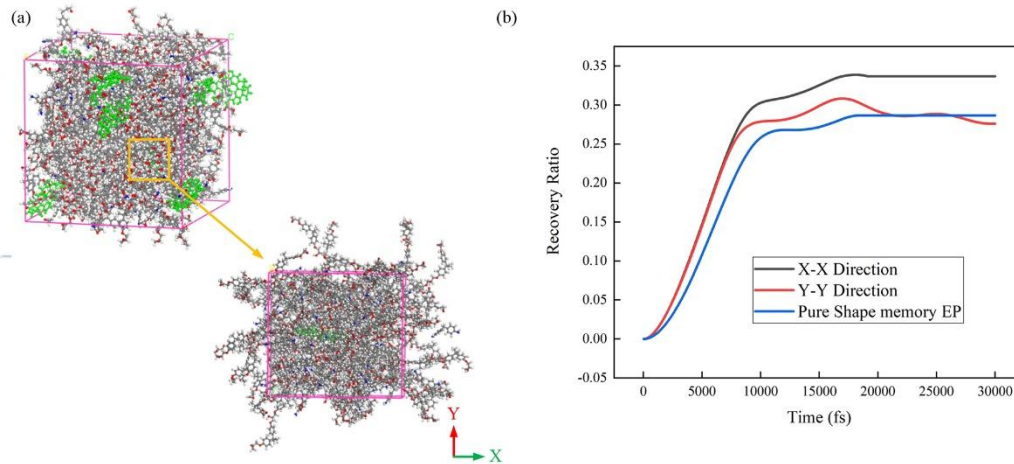


Fig. 13. The effect of GO agglomeration on shape recovery property.

#### 4.4.3 The influence of the direction of the GO sheets

As shown in Figure 14(a), a unit cell with one GO sheet was analyzed, and the shape recovery molecular dynamics simulation was performed in the X and Y directions. The simulation results show that the shape recovery effect of the unit cell along the X direction is better (see Figure 14(b)). The simulation results show that the shape recovery ratio is 33.67% at 30000 fs, which is 28.5% higher than that of pure shape memory EP. In the Y direction, the recovery ratio is 27.61%, which is 3.57% lower than that of pure shape memory EP. In addition, the shape recovery curves along X direction and Y direction coincide completely at the initial stage of shape recovery, which indicating that different directions do not affect the shape recovery speed of materials in the initial shape recovery stage.



408

409 Figure14. Schematic of (a) shape recovery, and (b) recovery effect in different directions.

## 410 5. Conclusions

411 In this paper, the shape recovery properties of shape memory GO/EP  
 412 composites were studied by preparing shape memory GO/EP composites  
 413 and establishing molecular dynamics simulation model. The results show  
 414 that the glass transition temperature of shape memory GO/EP composites  
 415 increases with the increase of GO content, and the shape memory  
 416 properties of shape memory GO/EP composites are improved. The main  
 417 conclusions are as follows:

418 (1) With the increasing of GO content, the shape retention ratio of  
 419 shape memory GO/EP composites decreases, while the shape recovery  
 420 ratio rises. The fast recovery interval is advanced, and the slow recovery  
 421 interval of initial recovery is shortened rapidly. The fast recovery interval  
 422 of shape memory GO/EP composites with 1.25 wt% GO is 30 s earlier  
 423 than that of pure shape memory EP.

424 (2) Through molecular dynamics simulation, it is found that the  
 425 aggregation of GO in the shape memory GO/EP composites reduces the



426 recovery performance. The shape recovery effect of shape memory  
427 GO/EP composites with 10 wt% GO content is 14.38% lower than that of  
428 uniform dispersion and 3.2% lower than that of pure shape memory EP.

429 (3) The simulation results indicate that the tensile recovery ratio  
430 perpendicular to the GO direction is 21.73% higher than that along the  
431 GO direction, while recovery in different directions does not affect the  
432 recovery ratio of the material in the initial shape recovery stage.

433

#### 434 **Author contribution statement**

435 **Long Chen:** Conceptualization, Data curation, Writing-review & editing,  
436 Methodology. **Yeqin Shen:** Formal analysis, Methodology,  
437 Writing-original draft. **Zhanqiang Liu:** Formal analysis, Methodology.  
438 **Qinghua Song:** Data curation, Writing-review & editing. **Chaozong Liu:**  
439 Conceptualization, Supervision.

440

#### 441 **Acknowledgements**

442 This work is supported by the Natural Foundation of Shandong Province  
443 (Grant No. ZR2019BEE068), and Natural Science Foundation of  
444 Guangdong Province (Grant No. 2020A1515111208). The authors thank  
445 the referees of this paper for their valuable and very helpful comments.

446

447

448 **References**

- 449 [1] Kong, D. Y.; Li, J; Guo, A. R.; Xiao X. L. High temperature  
450 electromagnetic shielding shape memory polymer composite. Chem.  
451 Eng. J. 2021, 408, 127365.
- 452 [2] Niels, V. H.; Filip E., D. P. Fast healing of polyurethane thermosets  
453 using reversible triazolinedione chemistry and shape-memory.  
454 Macromolecules 2018, 51, 3405-3414.
- 455 [3] Meurer, J.; Agudo, J. A. R.; Zechel, S.; Hager, M. D.; Schubert, U. S.  
456 Quantification of triple-shape memory behavior of polymers  
457 utilizing tension and torsion. Compos. Pt. A-Appl. Sci. Manuf. 2021,  
458 222, 2000462.
- 459 [4] Xiao, Y.; Zhou, S.; Wang, L.; Gong, T. Electro-active shape memory  
460 properties of poly( $\epsilon$ -caprolactone)/functionalized multiwalled carbon  
461 nanotube nanocomposite, ACS Appl. Mater. Interfaces 2010, 2,  
462 3506-3514.
- 463 [5] Uranbey, L.; Unal, H. I.; Calis G, Gumus OY, Katmer S, Karatas C.  
464 One-pot preparation of electroactive shape memory  
465 polyurethane/carbon black blend. J. Mater. Eng. Perform. 2021, 30,  
466 1665-1673.
- 467 [6] Du, L.; Xu, Z. Y.; Fan, C. J.; Xiang, G.; Yang, K. K.; Wang, Y. Z. A  
468 fascinating metallo-supramolecular polymer network with  
469 thermal/magnetic/light-responsive shape-memory effects anchored

- 470 by Fe<sub>3</sub>O<sub>4</sub> nanoparticles. *Macromolecules* 2018, 51, 705-715.
- 471 [7] Yu, X. J.; Zhou, S. B.; Zheng, X. T.; Guo, T.; Xiao, Y.; Song, B. T. A  
472 biodegradable shape-memory nanocomposite with excellent  
473 magnetism sensitivity. *Nanotechnology* 2009, 20, 235702.
- 474 [8] Li, Y.; Chen, H. M.; Liu, D.; Wang, W. X.; Liu, Y.; Zhou, S. B.  
475 PH-responsive shape memory poly(ethylene  
476 glycol)–poly( $\epsilon$ -caprolactone)-based polyurethane/cellulose  
477 nanocrystals nanocomposite. *ACS Appl. Mater. Interfaces*. 2015, 7,  
478 12988-12999.
- 479 [9] Defize, T.; Thomassin, J. M.; Ottevaere, H.; Malherbe, C. ; Eppe,  
480 G.; Jellali, R.; Alexandre, M.; Jerome, C.; Riva, R.  
481 Photo-cross-linkable coumarin-based poly( $\epsilon$ -caprolactone)  
482 for light-controlled design and reconfiguration  
483 of shape-memory polymer networks. *Macromolecules* 2019, 52,  
484 444-456.
- 485 [10] Wang, T. J.; Zhao, J.; Weng, C. X.; Wang, T.; Liu, Y. Y.; Han, Z. P.;  
486 Zhang, Z. A bidirectionally reversible light-responsive actuator  
487 based on shape memory polyurethane bilayer. *Compos. Pt. A-Apl.*  
488 *Sci. Manuf.* 202, 144, 106322.
- 489 [11] Leverant, C. J.; Zhang, Y. F.; Cordoba, M. A.; Leo, S. Y.; Charpota,  
490 N.; Taylor, C.; Jiang, P. Macroporous superhydrophobic coatings  
491 with switchable wettability enabled by smart shape memory

- 492 polymers. *Adv. Mater. Interfaces.* 2021, 8, 2002111.
- 493 [12] Chan, B. Y. Q.; Low, Z. W. K.; Heng, S. J. W.; Chan, S. Y.; Owh, C.;  
494 Loh, X. J. Recent advances in shape memory soft materials for  
495 biomedical applications. *ACS Appl. Mater. Interfaces.* 2016, 8,  
496 10070-10087.
- 497 [13] Ren, L. Q.; Li, B. Q.; Song, Z. Y.; Liu, Q. P.; Ren, L.; Zhou, X. L.  
498 Bioinspired fiber-regulated composite with tunable  
499 permanent shape and shape memory properties via 3d magnetic  
500 printing. *Compos. B Eng.* 2019, 164, 458-466.
- 501 [14] Alghamdi, S. S.; John, S.; Choudhury, N. R.; Dutta, N. K. Additive  
502 manufacturing of polymer materials: progress, promise and  
503 challenges. *Polymer* 2021, 13, 753.
- 504 [15] Hu, J. L.; Zhu, Y.; Huang, H. H.; Lu, J. Recent advances in shape  
505 memory polymers: structure, mechanism, functionality modeling  
506 and applications. *Prog. Polym. Sci.* 2012, 37, 1720-1763.
- 507 [16] Jian, W.; Wang, X. D.; Lu, H. B.; Lau, D. Molecular dynamics  
508 simulations of thermodynamics and shape memory effect in  
509 CNT-epoxy nanocomposites. *Compos. Sci. Technol.* 2021, 211,  
510 108849.
- 511 [17] Srivastava, S.; Biswas, A.; Senapati, S.; Ray, B.; Rana, D.; Aswal, V.  
512 K.; Maiti, P. Novel shape memory behaviour in IPDI based  
513 polyurethanes: influence of nanoparticle. *Polymer* 2017, 110,

- 514 95-104.
- 515 [18] Yu, Z. W.; Wang, Z. Q.; Li, H.; Teng, J. X.; Xu, L. D. Shape memory  
516 epoxy polymer (SMEP) composite mechanical properties enhanced  
517 by introducing graphene oxide (GO) into the matrix. *Materials* 2019,  
518 12, 1107.
- 519 [19] Dhand, V.; Mittal, G.; Rhee, K. Y.; Park, S. J.; Hui, D. A short review  
520 on basalt fiber reinforced polymer composites. *Compos. Part B* 2015,  
521 73, 166-180.
- 522 [20] Sliozberg, Y. R.; Kroger, M.; Henry, T. C.; Datta, S.; Lawrence, B.  
523 D.; Hall, A. J. A chattopadhyay computational design of shape  
524 memory polymer nanocomposites. *Polymer* 2015, 127, 123476.
- 525 [21] Idumah, C. I.; Odera, S. R. Recent advancement in self-healing  
526 graphene polymer nanocomposites, shape memory, and coating  
527 materials. *Polym -Plast. Technol. Mater.* 2020, 59, 1167-1190.
- 528 [22] Meng, Q. H.; Hu, J. L.; Zhu, Y. Shape-memory  
529 polyurethane/multiwalled carbon nanotube fibers. *J. Appl. Polym.  
530 Sci.* 2007, 106, 837-848.
- 531 [23] Deka, H.; Karak, N.; Kalita, R. D.; Buragohain, A. K. Biocompatible  
532 hyperbranched polyurethane/multi-walled carbon nanotube  
533 composites as shape memory materials. *Carbon* 2010, 48,  
534 2013-2022.
- 535 [24] Gopinath, S.; Adarsh, N. N.; Nair, P. R.; Mathew, S. Shape-memory

536 polymer nanocomposites of poly(epsilon-caprolactone) with the  
537 polystyrene-block-polybutadiene-block-polystyrene-tri-block  
538 copolymer encapsulated with metal oxides. ACS Omega 2021, 6,  
539 6261-6273.

540 [25] Jana, R. N.; Yoo, H. J.; Cho, J. W. Synthesis and properties of shape  
541 memory polyurethane nanocomposites reinforced with  
542 poly(e-caprolactone)-grafted carbon nanotubes. Fibers Polym. 2008,  
543 9, 247-254.

544 [26] Ashori, A.; Fallah, A.; Ghiyasi, M.; Rabiee, M. Reinforcing effects  
545 of functionalized graphene oxide on glass fiber/epoxy composites.  
546 Polym. Compos. 2018, 39, E2324-2333.

547 [27] Wang, C. C.; Zhao, Y. Y.; Ge, H. Y.; Qian, R. S. Enhanced  
548 mechanical and thermal properties of short carbon fiber reinforced  
549 polypropylene composites by graphene oxide. Polym. Compos. 2018,  
550 39, 405-413.

551 [28] Lee, C. G.; Wei, X. D.; Kysar, J. W.; Hone, J. Measurement of the  
552 elastic properties and intrinsic strength of monolayer graphene. Sci.  
553 2008, 321, 385-388.

554 [29] Yang, Q. R.; Zhang, Z. L.; Gong, X. F.; Yao, E. R.; Liu, T.; Zhang, Y.;  
555 Zhou, H. S. Thermal conductivity of graphene-polymer composites:  
556 implications for thermal management. Heat Mass Transfer 2020, 56,  
557 1931-1945.

- 558 [30] Koziol, M.; Jesionek, M.; Szperlich, P. Addition of a small amount of  
559 multiwalled carbon nanotubes and flaked graphene to epoxy resin. *J.*  
560 *Reinf. Plast. Compos.* 2017, 36, 640-654.
- 561 [31] Ligati, S.; Lavi, A. O.; Keyes, J.; Ziskind, G.; Regev, O. Enhancing  
562 thermal conductivity in graphene-loaded paint: Effects of phase  
563 change, rheology and filler size. *Int. J. Therm. Sci.* 2020, 153,  
564 106381.
- 565 [32] Kim, J. T.; Kim, B. K.; Kim, E. K.; Park, H. C.; Jeong, H. M.  
566 Synthesis and shape memory performance of polyurethane/graphene  
567 nanocomposites. *React. Funct. Polym.* 2014, 74, 16-21.
- 568 [33] Luo, X.; Wu, Y. P.; Guo, M. L.; Yang, X.; Xie, L. Y.; Lai, J. J.; Li, Z.  
569 Y.; Zhou, H. W. Multi-functional polyurethane composites with  
570 self-healing and shape memory properties enhanced by graphene  
571 oxide. *J. Appl. Polym. Sci.* 2021, 138, 50827.
- 572 [34] Xu, L.; Cui, L.; Li, Z.; Lu, H. H.; Qi, X. M.; Wang, W. J.; Jin, X. X.;  
573 Dong, Y. B.; Fu, Y. Q.; Jiang, W. B.; Ni, Q. Q. Thermodynamic  
574 coupling behavior and energy harvesting of vapor grown carbon  
575 fiber/graphene oxide/epoxy shape memory composites. *Compos. Sci.*  
576 *Technol.* 2021, 203, 108583.
- 577 [35] Ghosh, T.; Karak, N. Interpenetrating polymer  
578 network/functionalized-reduced graphene oxide nanocomposite: As  
579 an advanced functional material. *J. Appl. Polym. Sci.* 2021, 138,

- 580 50499.
- 581 [36] Wick, C. D.; Peters, A. J.; Li, G. Q. Quantifying the contributions of  
582 energy storage in a thermoset shape memory polymer with high  
583 stress recovery: A molecular dynamics study. *Polymer* 2021, 213,  
584 123319.
- 585 [37] Yang, H.; Zheng, X. R.; Sun, Y. G.; Yu, K.; He, M. C.; Guo, Y. F. A  
586 molecular dynamics study on the surface welding and shape memory  
587 behaviors of Diels-Alder network. *Comput. Mater. Sci.* 2017, 139,  
588 48-55.
- 589 [38] Zhang, X. J.; Yang, Q. S.; Leng, J. S. How graphene oxide affects  
590 shape memory properties and strength of  
591 poly(L-lactide-co-ε-caprolactone). *J. Intell. Mater. Syst. Struct.* 2020,  
592 31, 2152-6214.
- 593 [39] Amini, M.; Hasheminejad, H.; Montazeri, A. Experimentally guided  
594 MD simulation to enhance the shape memory behavior of  
595 polymer-based nanocomposites: Towards elaborating the underlying  
596 mechanism. *Compos. Pt. A-Appl. Sci. Manuf.* 2020, 138, 106055.



*Cover letter*

Long Chen  
School of Mechanical Engineering, Shandong University  
Room 1210, The Innovation Building, No. 250061 Jingshi Road, Lixia District, Jinan, China

18/08/2021

Dear Chief-Editor,

We wish to submit an original research article entitled “**Investigation of the effects of graphene oxide on thermodynamic performance of shape memory GO/EP composites**” for consideration by **Journal of Materials Science & Technology**.

We confirm that this work is original and has not been published elsewhere, nor is it currently under consideration for publication elsewhere.

In this paper, we prepared shape memory GO/EP composite and the shape recovery properties of shape memory GO/EP composites were studied by preparing shape memory GO/EP composites and establishing molecular dynamics simulation model. This is significant because the heat transfer and shape memory performance of the anti-/deicing structure plays a significant role, which directly influencing the anti-/deicing efficiency and flight safety.

We believe that this manuscript is appropriate for publication by **Journal of Materials Science & Technology** because it matches the scope of this journal, which focus on thermodynamics of composite materials.

We have no conflicts of interest to disclose.

Please address all correspondence concerning this manuscript to me at 812612937@qq.com

Thank you for your consideration of this manuscript. We look forward to hearing from you.

Sincerely,

Long Chen

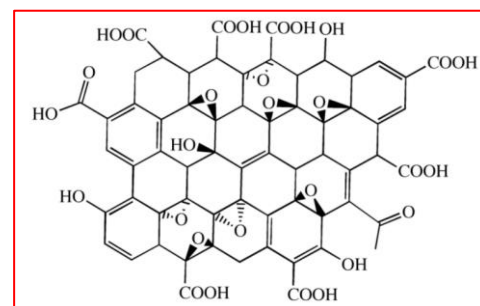
**Declaration of interests**

The authors declare that they have no known competing financial interests or personal relationships that could have appeared to influence the work reported in this paper.

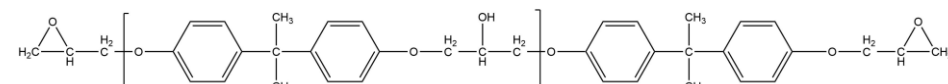
The authors declare the following financial interests/personal relationships which may be considered as potential competing interests:

HIGHLIGHTS:

- A shape memory GO/EP composite was prepared by introducing GO sheets into shape memory EP and the molecular dynamics model was established.
- The anti-icing time of the shape memory GO/EP composites was shortened by 18.84s, and the anti-icing efficiency was increased by 49.90%.
- The deicing time of samples with shape memory function decreased from 136 s to 45 s, and the deicing efficiency increased by 66.91%.
- The GO doping content has a direct effect on the anti-/deicing performance of the shape memory GO/EP composites.



Graphene oxide +



Epoxy resin E51

